Metabolic Engineering 92 (2025) 148–160

Contents lists available at ScienceDirect

Metabolic Engineering

journal homepage: www.elsevier.com/locate/meteng

Microbial production of creatine using growth-coupled selection systems

Jinbei Li [a,2,3], Simon R. Krarup [a,2,3], Pascal Pieters [a,2], Tobias B. Alter [a,1], Paul Jacottin [a], Josefin Johnsen [a], Elsayed T. Mohamed [a], Thomas Harris [b], Linda Ahonen [a], Khem Bahadur Adhikari [a], Bernhard O. Palsson [a,b], Adam M. Feist [a,b,*], Lei Yang [a,**]

[a] The Novo Nordisk Foundation Center for Biosustainability, Technical University of Denmark, Søltofts Plads, Building 220, 2800 Kgs. Lyngby, Denmark
[b] Department of Bioengineering, University of California, 9500 Gilman Dr. #0412, La Jolla, CA, San Diego, 92093-0412, USA

A B S T R A C T

Creatine is an important energy storage molecule produced exclusively in vertebrates and is crucial for muscle development. It is particularly valuable as a food supplement, especially for plant-based diets. Here, we present an alternative to chemical synthesis by developing a biosynthetic process using an *Escherichia coli* cell factory expressing a heterologous pathway. We employed a model-driven growth-coupled selection approach combined with adaptive laboratory evolution to overcome metabolic bottlenecks in the heterologous synthesis of creatine. We developed a novel growth-coupling strategy to optimize an important glycine amidinotransferase step guided by genome-scale modeling. We also improved creatine tolerance of *E. coli* by adaptive evolution. Several design-build-test-learn cycles of evolution and selection resulted in a 58 % increase in titer over the baseline strain from glycine and arginine. This study highlights the advantage of combining production with growth for efficient cell factory generation driven by evolutionary engineering and computational biology.

1. Introduction

Creatine is a molecule that is used as an energy storage and buffering system in vertebrates through the creatine/phosphocreatine system, where phosphate groups are enzymatically transferred between ATP and creatine (Bonilla et al., 2021). The molecule plays substantial roles in muscle development and neurophysiological performance (Kaviani et al., 2020). Human endogenous creatine production (~1 g/d) meets only half the daily requirement (~2 g/d), thus needs to be supplemented (Brosnan and Brosnan, 2016; Juneja et al., 2024). However, creatine is only found in animal-based food, underscoring the importance of alternative creatine supplementation for plant-based diets (Balestrino and Adriano, 2019; Benton and Donohoe, 2011; Blancquaert et al., 2018; Bonilla et al., 2024; Edison et al., 2013; Francaux and Poortmans, 1999; Juneja et al., 2024; Korovljev et al., 2021; Prokopidis et al., 2023).

The creatine currently available on the market is produced through chemical synthesis, which is an energy intensive process dependent on fossil-based raw materials (Güthner and Mertschenk, 2006; Pischel and Gastner, 2007). Moreover, one intermediate, cyanamide, poses a risk of food contamination due to residual cyanamide derivatives (Moret et al., 2011) and their removal increased the cost of downstream process significantly (Li et al., 2024). Here we aim to produce creatine using *Escherichia coli* as a cell factory as an alternative sustainable solution to replace the existing chemical synthesis process.

In vertebrates, creatine is synthesized from arginine and glycine in two enzymatic steps: 1) glycine amidinotransferase (GAT) converts arginine and glycine into ornithine and guanidinoacetate (GAA); 2) guanidinoacetate methyltransferase (GAMT) adds a methyl group to GAA using cofactor S-adenosylmethionine (SAM), forming creatine (Brosnan and Brosnan, 2016). GAA itself is often used as an additive in animal feed or as a supplement to boost creatine levels in humans (Edison et al., 2013). A one-step conversion from GAA to creatine has been implemented in a bacterial host (Li et al., 2024). Here, we assembled the full pathway in *Escherichia coli* and utilized growth-coupling strategies to optimize the enzymes and host tolerance.

The goal of growth-coupling is to engineer the target enzyme's activity to be essential for cell growth, such that higher enzyme activity leads to better growth (Orsi et al., 2021). This advantageous approach allows high-throughput screening and selection of improved variants by growth, eliminating expensive chemical analytics. Growth-coupling can

* Corresponding author. The Novo Nordisk Foundation Center for Biosustainability, Technical University of Denmark, Søltofts Plads, Building 220, 2800 Kgs. Lyngby, Denmark.
** Corresponding author.
E-mail addresses: afeist@ucsd.edu (A.M. Feist), leiya@biosustain.dtu.dk (L. Yang).
[1] Present address: Institute of Applied Microbiology, Aachen Biology and Biotechnology, RWTH Aachen University, Worringerweg 1, 52074 Aachen, Germany.
[2] Present address: Enzidia ApS, Kgs. Lyngby, DK2800, Denmark.
[3] Equal contribution.

https://doi.org/10.1016/j.ymben.2025.07.009
Received 12 February 2025; Received in revised form 2 July 2025; Accepted 23 July 2025
Available online 23 July 2025

be achieved by rewiring the metabolic network or changing the culture media so that the target reaction is essential for growth in the defined condition (Guzmán et al., 2015; Luo et al., 2019, Luo et al., 2020; Orsi et al., 2021; Wang et al., 2019). Genome-scale metabolic models can be leveraged by appropriate optimization algorithms to derive genetic engineering strategies and medium conditions that enforce growth-coupling (Alter and Ebert, 2019; Feist et al., 2010; Hassani et al., 2024; Jensen et al., 2019; Schneider et al., 2021). Previously, we developed a growth-coupling strategy for SAM-dependent methyltransferases and successfully applied it to pathway optimization (Luo et al., 2019). Additionally, a range of algorithms and models have been developed to design growth-coupled strains using different strategies (Guzmán et al., 2015; Li et al., 2023; Orsi et al., 2021; Wang et al., 2019).

In this work, we constructed a creatine biosynthesis pathway in *E. coli* by heterologously inserting GAT and GAMT and feeding glycine and arginine (Fig. 1A). Further, we created a growth coupling strategy for optimizing GAT, a rate-limiting step, resulting in a 58 % improvement of creatine titer over the parent strain. The growth coupling strategy was designed using a genome-scale model. However, when we implemented the design in experiments, we came across a few unexpected challenges. Eventually the design was modified to have a lower coupling strength, which led to successful selection of improved GAT variants (Fig. 1B). Moreover, we noticed product inhibition when creatine is produced intracellularly. We used adaptive laboratory evolution (ALE) (Sandberg et al., 2019) to increase the creatine tolerance level of *E. coli,* leading to a strain producing over 100 mg/L creatine from whole-cell bioconversion.

2. Results

2.1. Creatine biosynthesis pathway assembly in E. coli

The biosynthesis of creatine from L-arginine and glycine requires the heterologous enzyme glycine amidinotransferase (GAT, EC 2.1.4.1) to produce guanidinoacetate (GAA) and guanidinoacetate N-methyltransferase (GAMT, EC 2.1.1.2) for the subsequent methylation to creatine (Fig. 1A). We selected eight GAT and four GAMT enzyme sequences from UniProt (Bateman et al., 2023), covering a large diversity both in their sources and the sequences. The enzyme sequences were subsequently codon-optimized for expression in *E. coli* and cloned into expression vectors.

The creatine biosynthetic pathway was established in *E. coli* BW25113 after verifying that extracellular supplementation with GAA and creatine did not result in significant growth inhibition within solubility limits (Supplementary Fig. 1a and b). We constructed co-expression plasmids containing both GAT and GAMT for an initial evaluation of creatine production levels in *E. coli*. To this end, a single GAMT variant (GAMT4) was combined into co-expression cassettes with 6 different GAT variants and GAT8 showed the best production

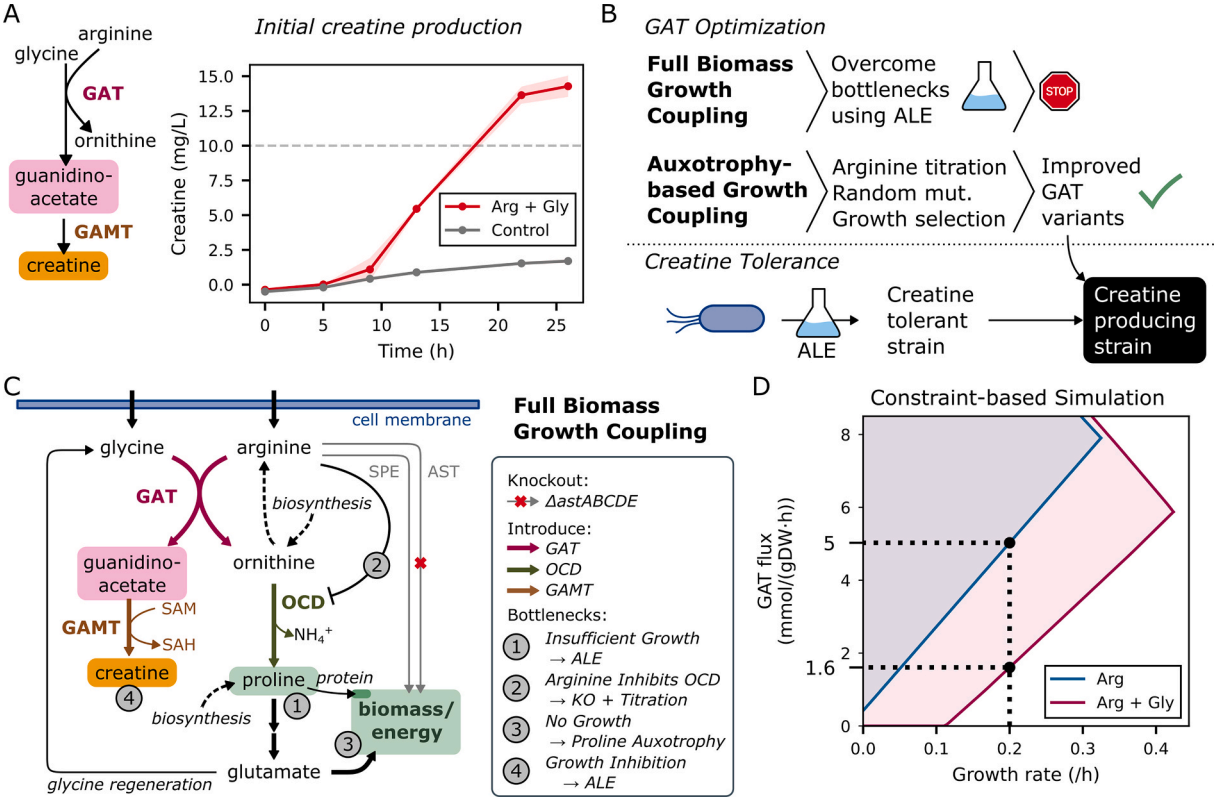

Fig. 1. Creatine production in *Escherichia coli* and GAT growth coupling. A) Reactions involved in the production of creatine from glycine and L-arginine. Creatine production over time for *E. coli* BW25113 expressing GAMT4 and GAT8, with (red) or without addition of arginine and glycine (grey). The dashed grey line indicates the detection limit of the creatine quantification assay. B) Overview of the workflow for optimization of creatine production. C) A computationally designed growth-coupling design for GAT, based on the conversion of L-ornithine to L-proline and subsequently to biomass and energy. Major challenges and solutions during experimental implementation of the design are listed in the box. Creatine inhibition is not directly associated with the GAT-coupling but needed to be solved to enhance creatine production. D) Feasible flux spaces for GAT activity versus growth rate for the GAT selection system using arginine as the carbon source (blue) and co-fed with glycine (red). Minimum required fluxes for GAT are indicated for a growth rate of 0.2 (/h). GAT: glycine amidinotransferase, GAMT: guanidinoacetate N-methyltransferase, SAM: S-Adenosyl-L-Methionine, SAH: S-adenosyl homocysteine, Arg: L-arginine, Gly: glycine, OCD: ornithine cyclodeaminase, SPE: arginine decarboxylase/agmatinase pathway, AST: L-arginine succinyltransferase pathway. (For interpretation of the references to colour in this figure legend, the reader is referred to the Web version of this article.)

(Supplementary Fig. 1c). Introduction of the combined creatine production pathway into *E. coli* strain BW25113 resulted in accumulation of creatine in the supernatant (Fig. 1A), with significantly improved production by addition of 0.2 % glycine and 0.2 % arginine.

2.2. Overview of creatine production optimization

After initial pathway assembly, we focused on optimization of two major obstacles of creatine production – GAT enzyme and creatine toxicity.

First, we designed a growth-coupling strategy to improve the GAT enzyme, through coupling growth to the by-product ornithine. Ornithine can be incorporated into biomass through proline (Fig. 1C). The details of the design will be explained in the next section. During the implementation of the coupling design, we encountered a few bottlenecks, including insufficient growth on ornithine and proline, and arginine inhibition of the ornithine cyclodeaminase (OCD), a key enzyme for the coupling. Eventually, we modified the design to use ornithine generated by the creatine pathway to complement proline auxotrophy, instead of full biomass growth. This weaker coupling was successfully implemented and led to screening of better GAT variants.

Second, we found creatine is toxic when produced intracellularly (see later section), although it did not show growth inhibition when added externally (Supplementary Fig. 1b). To solve this bottleneck, we employed ALE to increase the tolerance, which allows for creatine production of higher titers. The details of this ALE run will be explained later. The overview of the optimization process is illustrated in Fig. 1B and C.

2.3. Design 1 – coupling GAT activity to growth

To improve the GAT enzyme activities, we opted to couple the GAA biosynthesis pathway to growth, enabling high-throughput selection and evolution experiments to increase production. Finding strategies that strictly couple a metabolic functionality to growth remains a challenging task due to the inherent complexity and redundancy of metabolic networks. Constraint-based metabolic model approaches have been successfully used to derive growth-coupling strain designs by harnessing their dense biochemical and phenotypic knowledge (Feist et al., 2010; Jensen et al., 2019). We utilized an automated workflow based on the gcOpt algorithm to find enzyme selection systems for GAT (Alter et al., 2024). Here, we did not focus on the second enzyme in the pathway, GAMT, but note that an existing coupling strategy could be used to improve this enzyme (Luo et al., 2019).

The computational design aimed to couple cell growth with amidinotransferase activity by engineering a metabolic network in which arginine and glycine serve as the sole carbon sources. In this design, GAT converts these substrates into ornithine, thereby linking creatine precursor formation to ornithine synthesis. By heterologously expressing ornithine cyclodeaminase (OCD) and eliminating competing ornithine sinks, proline synthesis and therefore GAT activity become essential for growth. This L-ornithine is used as both a carbon and energy source through a conversion to L-proline by OCD (Fig. 1 C). The design is thus based on the model prediction that *E. coli*, after metabolic readjustments, could efficiently grow on L-proline as the sole carbon and energy source. It was crucial that there exist no alternative L-arginine utilization pathways that circumvented the amidinotransferase reaction in this enzyme selection system. Thus, two main pathways that could enable escape from the designed flux pattern were identified via modeling: arginine degradation II encoded by *astABCDE* and putrescine biosynthesis I encoded by *speAB*, which are knockout targets to enable growth-coupling.

In this GAT selection system (Fig. 1C), an increase in GAT activity would lead to higher growth rates, within an operating window where GAT activity is a bottleneck for arginine utilization. An *in silico* analysis of the selection system design using flux balance analysis confirmed that GAT activity was enforced for any given growth rate (Fig. 1D). The maximum growth rate was predicted at 0.32/h for an L-arginine uptake rate of 8 mmol gDW^{-1}/h corresponding to a carbon uptake rate of 48 C-mmol gDW^{-1}/h. To partially relieve the inflicted metabolic burden on the mutant cell, glycine, the second GAT substrate besides L-arginine, could be co-fed. When employing the same total carbon uptake rate for L-arginine, cofeeding glycine and L-arginine at an equal molar ratio (6 mmol gDW^{-1}/h) increased the maximum growth rate to 0.42/h while preserving growth-coupling of GAT, above a minimum growth rate. Altogether, these simulations confirm the feasibility of the GAT growth-coupling design and establish a method to alleviate flux requirements by co-feeding.

2.4. Establishment of design 1 for GAT growth-coupling in E. coli

The GAT selection system requires the OCD enzyme and all downstream reactions to be able to carry sufficient metabolic flux to enable growth on ornithine, while the selection pressure is left at the GAT reaction. We therefore selected a synthetic OCD variant ($OCD_{K205G/M86K/T162A}$ from *Pseudomonas putida*, OCDv1) for implementation into the selection system, since it was reported to have a 2.85-fold increased catalytic efficiency compared to the WT (OCD_{WT}) (Long et al., 2020). We subsequently performed growth tests on all relevant carbon sources using *E. coli* BW25113 strains with and without OCDv1, *speA* knockout and *astA* knockout, respectively (Supplementary Table S5). Some growth was observed when strains were grown on proline, which supports the possibility of using proline as intermediate for biomass to enable selection system. When supplying ornithine to a strain expressing OCDv1, no growth was observed. This could be explained by the already inefficient growth on proline, insufficient OCD activity, or a combination thereof. Additionally, when feeding arginine and glycine, wildtype BW25113 and *ΔspeA* strains can grow slightly, but the AST knockout showed no growth. This indicates that the AST pathway could bypass the selection system. Consequently, *ΔastA* strain was used in the subsequent experiments.

We sought to verify whether the observed lack of growth on ornithine could be explained by low OCDv1 activity. Therefore, a proline auxotroph (*ΔproB*) strain (SDT640) was employed, such that when ornithine is provided, an active OCD converts ornithine into proline to rescue cell growth. In most cases, however, OCDv1 could not restore growth of the proline auxotroph when a combination of ornithine and glucose was supplemented (Fig. 2A). However, with extended incubation time, one mutant arose at the late stage of the cultivation, $OCD_{K205G/M86T/T162A}$ (OCDv2), which showed better growth than OCDv1 and was used for later experiments (Fig. 2A).

2.5. Improving growth on proline and ornithine

With more potent OCD candidates identified, the challenge of limited growth of the engineered *E. coli* on proline remained (Table S5). It was not immediately obvious which enzymatic step was the limiting factor for proline-based growth, therefore we chose to use adaptive laboratory evolution (ALE) to overcome the growth challenge on proline and ornithine. We designed 3 ALE experiments. First, to improve growth on proline, we evolved Δ*astA* strain in the presence of proline and glycerol as helper substrate (Materials and Methods, Proline_ALE). The concentration of glycerol decreased at each passage using a process controlled weaning approach (Guzmán et al., 2019). After several passages, growth on proline was significantly improved for both BW25113 and the Δ*astA* strain, with growth rates above 0.2/h (Fig. 2B).

After obtaining an efficient population growing on proline, we transformed a plasmid pool containing a mutagenesis library made from OCD_{WT} to the Proline_ALE end point population, and screened the library on ornithine growth (Materials and Methods). An improved variant was identified containing four mutations (R65H, R184H, A185V, R244H; OCDv4) with respect to OCD_{WT}. We further optimized the

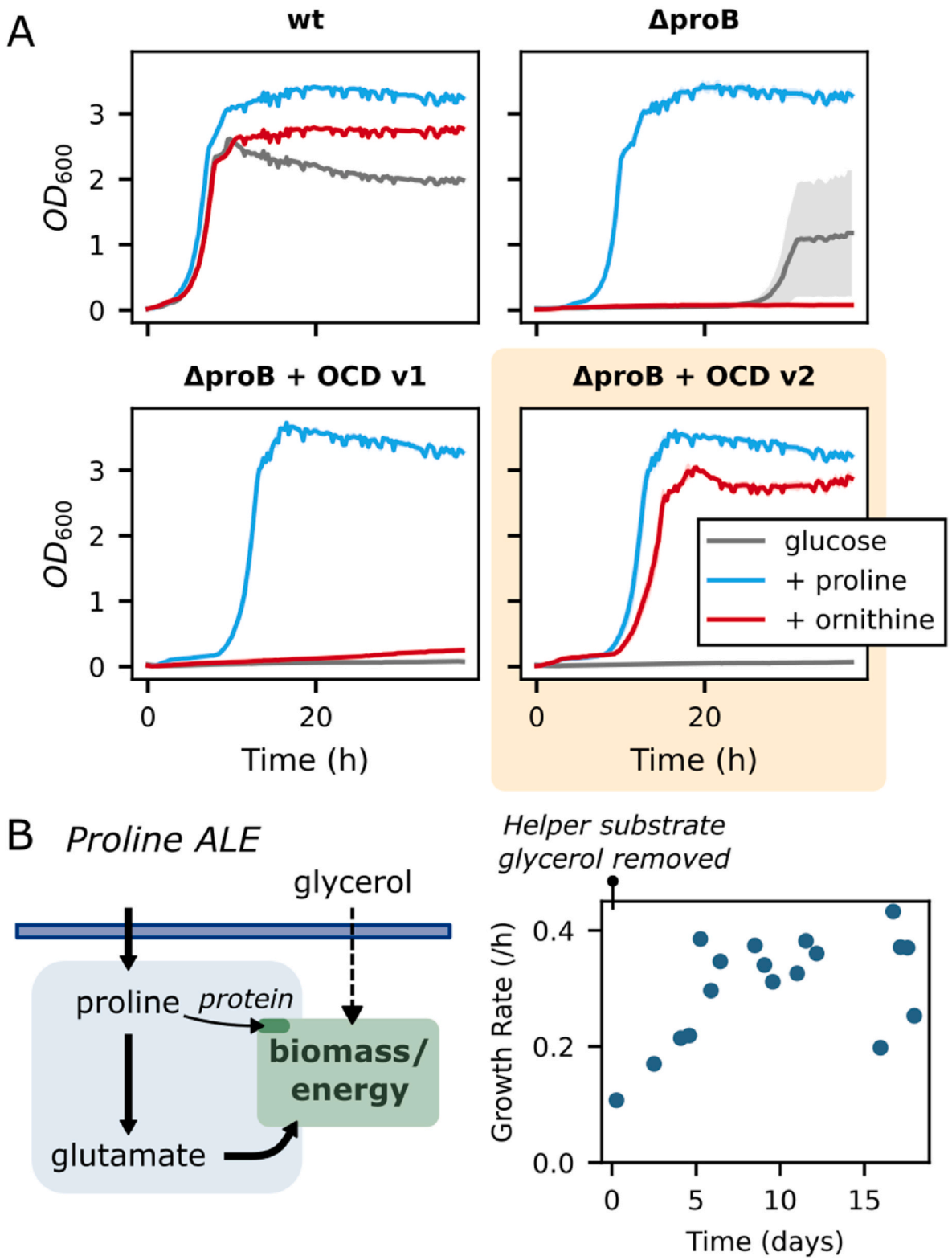

Fig. 2. Improvement of the conversion from proline to biomass. A) The activity of two OCD variants was tested by assessing their ability to rescue proline auxotrophy. Glucose, proline, and ornithine were supplemented at 0.2 %. B) Growth rate during the proline-ALE experiment using ΔastA (SDT854), after the helper substrate glycerol was completely removed from the experiment.

expression of this OCD variant by promoter and ribosome binding sites engineering, resulting in SDT969 for the follow-up experiments.

In parallel, we also attempted to achieve growth directly on ornithine through ALE, using a Δ*astA* strain carrying a plasmid expressing OCDv2 (SDT652). We performed ALE by feeding ornithine alone (Materials and Methods, Ornithine ALE) or co-feeding proline and ornithine by reducing concentration of glycerol (Proline-Ornithine ALE). Only Proline-Ornithine ALE resulted in one variant that led to growth on ornithine (OCDK205G/M86M/T162A, OCDv3).

2.6. GAT selection design 1 failure due to OCD inhibition by arginine

With a suitable GAT selection system strain determined, we continued to test growth coupling of GAT. We constructed a random mutagenesis library based on GAT8 and transformed it into SDT969 containing OCDv4 (Methods). However, after selection using arginine and glycine as the sole carbon sources, no growth was observed.

We first explored whether intracellular GAA could be the cause of the failure of the coupling. Although GAA was shown not to be toxic when added in the media (Supplementary Fig. 1a), it can still inhibit growth when accumulated intracellularly. This hypothesis was tested by growing SDT969 and SDT941 (a proline auxotroph, Δ*proB* + OCD_{WT}) strains transformed with GAT8 in permissive growth conditions (0.2 % glucose for SDT969, 0.2 % glucose and 0.1 % proline for SDT941), with or without the supplementation of arginine and glycine. The strains are not dependent on arginine and glycine for carbon and energy under these conditions, which enables the detection of growth inhibition by GAA when arginine and glycine are supplemented to the GAT8 bearing strains. However, we did not observe any growth defect when arginine and glycine were supplemented (Fig. 3A and B). This indicates that, even if GAA is accumulated in the cell, it is not disruptive to the selection system.

Another potential reason for the failure of the growth-coupling could be the inhibition of the heterologous OCD enzyme by a metabolite. To investigate this, we designed growth experiments that studied the effects of arginine and glycine supplementation on SDT969 (ALE isolate grows on ornithine, OCDv4) (Fig. 3A) and SDT941 (ΔproB, OCD_{WT} (Fig. 3B). In both cases, conversion of ornithine to proline by OCD is a requirement for growth, which enables the detection of inhibitory effects of arginine or glycine on OCD. We observed that arginine significantly inhibits

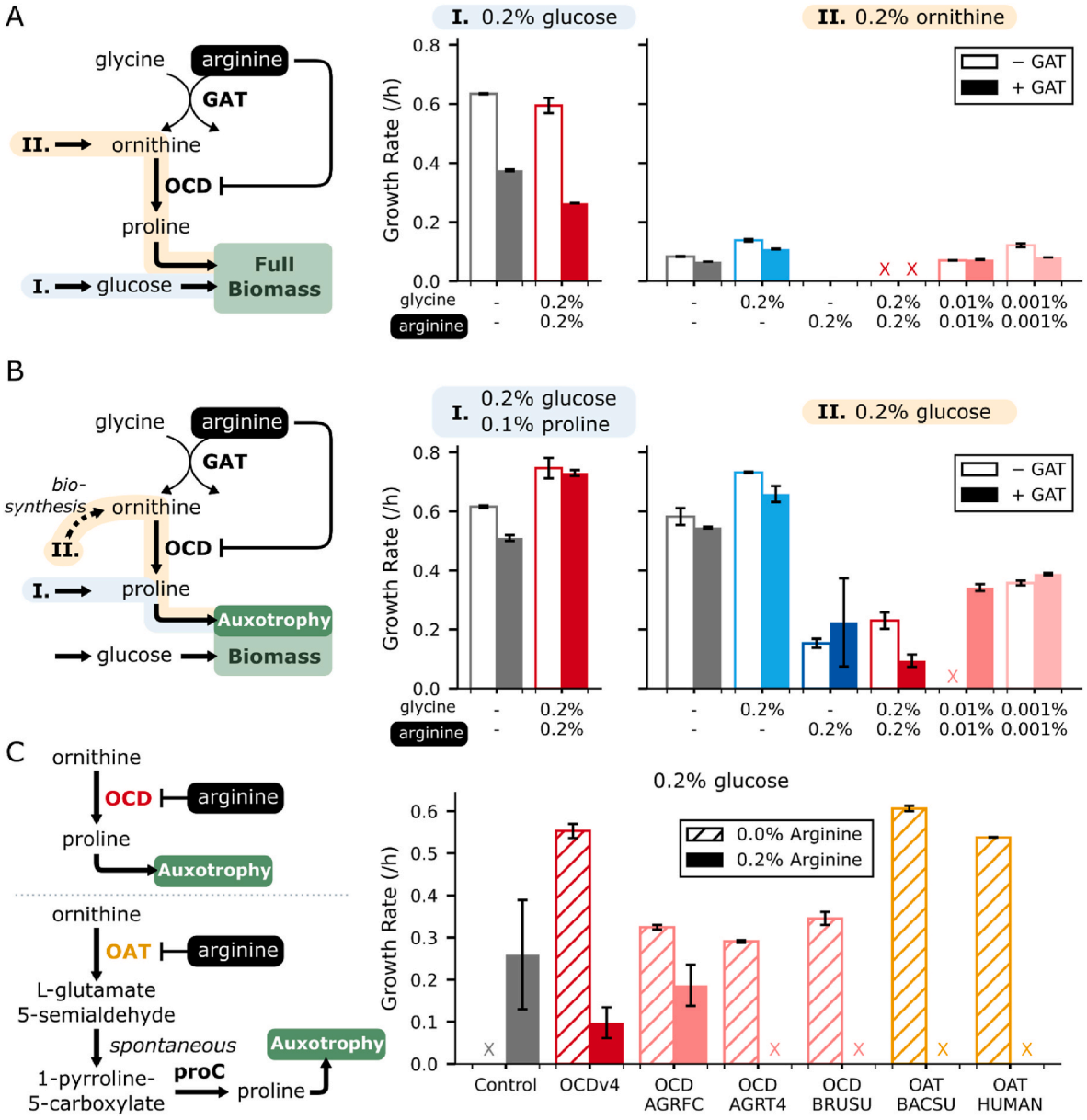

Fig. 3. Inhibition of growth by arginine. A) Growth rates of ornithine utilizing strain (via OCD) with (SDT989) or without (SDT969) GAT in various arginine and glycine concentrations. Biomass is either generated from glucose (I) or ornithine (II). Increasing arginine concentration leads to stronger inhibition of when ornithine was fed (OCD conditional essential), but no effect on glucose-based growth. B) Growth rates of a Δ*proB* strain expressing OCD with (SDT981) or without GAT (SDT941) in various arginine and glycine concentrations. Proline is either directly provided (I) or generated endogenously from glucose (II). Increasing the arginine concentration leads to stronger growth inhibition when proline needs to be produced from endogenous ornithine. C) Growth rates for strains expression three additional OCD and two OAT variants (SDT1043-47, SDT1051-53) in the presence and absence of arginine.

growth when OCD is conditional essential, with this effect becoming more pronounced as arginine concentrations increase from 0.001 % to 0.2 % (Fig. 3A and B). In contrast, the level of inhibition did not appear to depend on glycine supplementation, and no growth inhibition was seen when 0.2 % glycine was supplemented without arginine. The strains with GAT expression showed similar trends (Fig. 3A and B). It can therefore be concluded that the OCD enzyme used in these experiments was inhibited by arginine. Similar phenomena were previously reported for some OCD homologs in an early enzymology study (Schindler et al., 1989). We hypothesize that due to the highly similar molecular structures of ornithine and arginine, arginine can bind in the substrate binding site of OCD and block ornithine from being converted to proline.

We attempted to find alternatives to OCDv4 that would not suffer from arginine inhibition by constructing a small library of OCD variants of different origins and two ornithine aminotransferases (OAT). OAT converts ornithine to pyrroline-5-carboxylate, a precursor of proline in *E. coli*, and could therefore be a substitute for OCD activity. We cloned 5 more OCD/OAT variants, and they are all active, indicated by growth rescue of Δ*proB* in the absence of proline (Fig. 3C). However, all variants still suffered from apparent inhibition by arginine. We further performed selection from the OCD mutagenesis library, but also failed to identify a mutant escaping the arginine inhibition (Supplementary Fig. S2). These results indicate that cross-recognition of arginine is an inherent property of the catalytic mechanisms for similar enzymes.

In conclusion, after solving the bottlenecks of OCD activity and growth on proline, our attempt at building a growth-coupled GAT selection system still failed due to arginine inhibition of OCD. We then looked for a modified design and implementation with lower selection pressure.

2.7. Design 2 – A GAT selection system based on proline auxotrophy

The inhibition of OCD by arginine posed a major challenge for the originally designed selection system. A high concentration of arginine was required to support the full biomass and energy needs of the cell. Yet, such a high level of arginine would also mean strong inhibition of

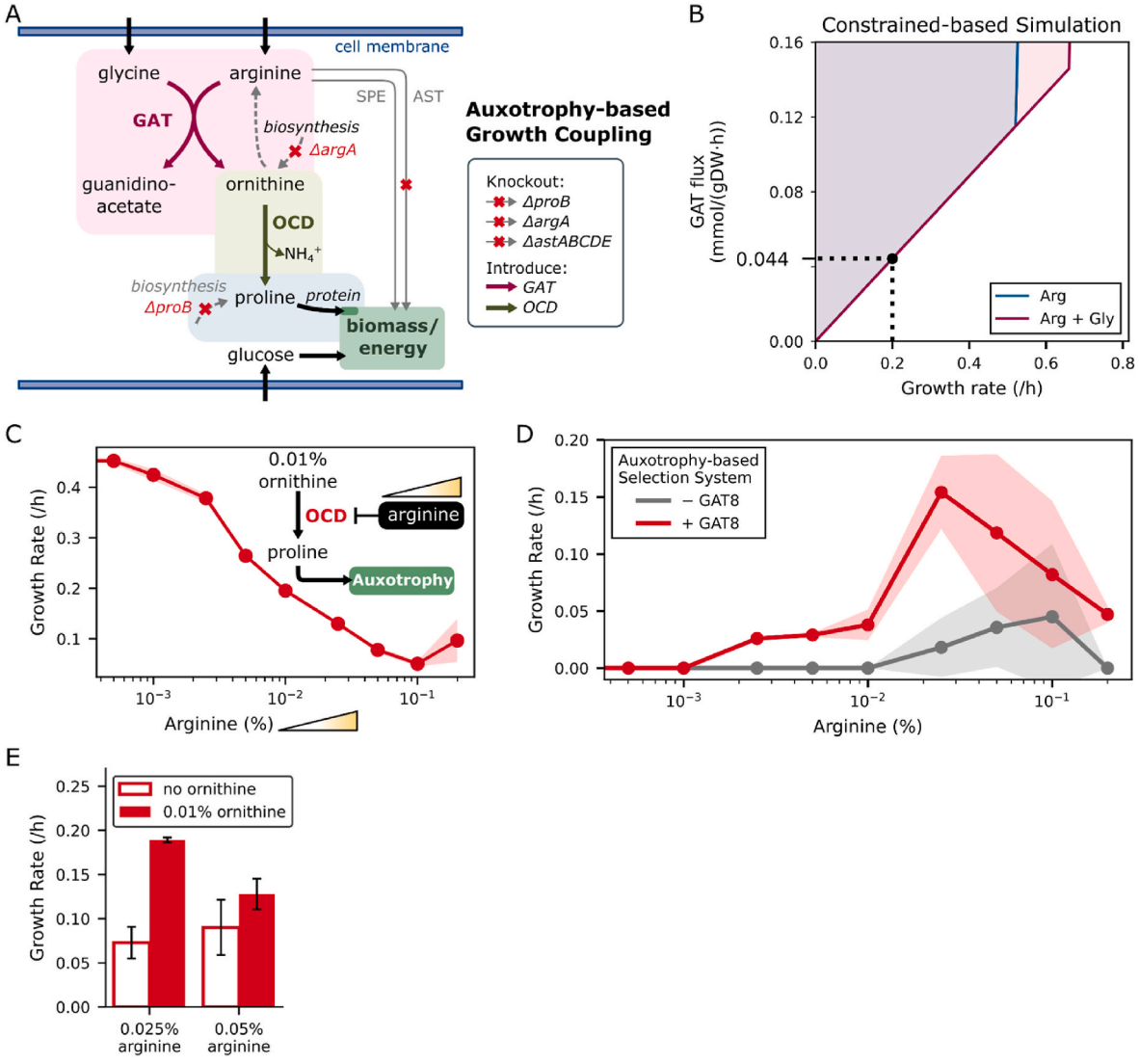

Fig. 4. Proline auxotrophy-based selection system. A) Design of the auxotrophy-based selection system. The deletion of *argA* eliminates intracellular synthesis of ornithine so ornithine can only be produced from arginine via GAT. B) Feasible GAT activity versus growth rate planes for the GAT selection system using arginine as the carbon source (blue) and co-fed with glycine (red). Minimum required fluxes for GAT are indicated for a growth rate of 0.2/h. C) Inhibition effects of OCDv4 (SDT1066) by arginine for a concentration gradient. D) Growth rates for the auxotrophy-based selection system with (SDT1127) and without (SDT1130) GAT8 for a range of arginine concentrations (black arrow: 0.025 %, grey arrow: 0.05 %). The data represents mean±standard deviation (shaded) of triplicates. E) Addition of ornithine to the selection system with GAT8 and 0.025 % or 0.05 % arginine leads to an increase in growth rate. The data represents mean±standard deviation of triplicates. (For interpretation of the references to colour in this figure legend, the reader is referred to the Web version of this article.)

OCD, an essential step for growth-coupling. Since our efforts to reduce the inhibitory effect of arginine were unsuccessful, we shifted our focus to modify the coupling strategy requiring considerably lower concentration of arginine. This can be achieved by coupling GAT activity to the relatively low cellular proline requirement in a proline auxotroph, instead of full biomass and energy (Fig. 4A). In this modified design, additional to OCD expression and AST pathway knockout, the proline biosynthesis pathway is knocked out (Δ*proB*) to introduce the auxotrophy and the biosynthesis of ornithine from the main carbon source is prevented (Δ*argA*) to ensure that the sole source for ornithine is provided by the GAT step. Computational analysis of this design using flux balance analysis revealed that GAT activity was indeed growth-coupled, but with up to two orders of magnitude lower flux requirements at a growth rate of 0.2/h (Fig. 4B) compared to the initial growth-coupling design (Fig. 1D).

The auxotrophy-based selection system was implemented in the previously used proline auxotroph Δ*proB* by the sequential introduction of Δ*argA* and Δ*astABCDE*, followed by transformation with a plasmid containing OCDv4. The resulting strain, SDT1066 (Δ*proB* Δ*argA* Δ*astABCDE* + OCDv4), is an auxotroph for both proline and arginine, but can synthesize both arginine and proline when ornithine is available.

To determine the operating window of the auxotrophy-based selection system, the strain was assessed under various conditions. We observed that the selection strain SDT1066 reached a maximum OD_{600} when ornithine is supplemented at 0.02 %, which is an indication of the cellular needs for both arginine and proline (Supplementary Fig. 4A. Similarly, we estimated the arginine requirement to be approximately 0.005 %, based on the maximum OD_{600} observed when growing a Δ*argA* Δ*astABCDE* strain with a range of arginine concentrations (Supplementary Fig. 4B). In addition, we sought to profile the inhibitory effects of arginine on OCDv4 as a function of arginine concentration in the novel selection system. At a fixed ornithine concentration of 0.01 %, arginine starts to severely inhibit growth of SDT1066 from 0.005 %, with a strong correlation between growth inhibition and arginine concentration (Fig. 4C). Finally, we assessed the growth of strain SDT1066 and strain SDT1127 (SDT1066 with GAT8) across various arginine concentrations (Fig. 4D). With GAT8, low arginine (<0.025 %) caused insufficient growth due to limited arginine and proline. This observation aligns with metabolic model predictions indicating that growth is strictly coupled to GAT-mediated arginine conversion (Fig. 1D). High arginine (>0.05 %) slowed growth by inhibiting OCDv4. Without GAT8, growth was significantly lower for any arginine concentration, suggesting that GAT activity aids growth by converting arginine and relieving OCD inhibition. This observation enables proline auxotrophy-based selection by externally adjusting the arginine concentration.

We simulated the effect of an improved GAT variant in the selection system to verify that cells with improved variants would indeed gain a selective advantage. Firstly, we studied the effect of an increased ornithine concentration, which simulates improved conversion of arginine and glycine by GAT. We grew the selection strain with GAT8 supplemented with 0.025 % or 0.05 % of arginine, with or without 0.01 % ornithine, and observed that additional ornithine indeed led to improved growth for both arginine concentrations (Fig. 4E). This indicated that at the current GAT8 expression level (pSC101-J23100-RBSU058-GAT8, pSD242), higher GAT activity can potentially improve growth. We further optimized the GAT expression level by varying promoter and RBS strengths (Supplementary Fig. 5).

2.8. GAT selection using proline auxotrophy

Having established an operating window for the proline auxotrophy-based selection system, we set out to perform selection on a library of GAT variants and improve GAA production rates (Fig. 5A). An error-prone PCR library of GAT8 under control of different promoters and RBS was constructed and transformed into the selection strain (SDT1066, ΔproB ΔargA ΔastABCDE + OCDv4). Selection was carried out by growing in M9 with glucose and 0.05 % arginine (Materials and Methods). Three GAT8 variants were found at the end of the growth selection, including GAT8_v1 containing M175T, Q211L and R232G, GAT8_v2 containing G25E, S181N and R232G, as well as GAT8_v3 containing M182L and G281D. Using AlphaFold3 (Abramson et al., 2024) and PyMOL, the locations of these mutations were visualized on predicted secondary protein structures in Supplementary Fig. 9. The AlphaFold model suggests that all three variants have at least one mutation in the same predicted alpha helix. The predicted structure of all three variants also included a change in the shape of the substrate binding pocket (Supplementary Fig. 10) compared to the predicted wild-type structure. These shared features could indicate that their distinct mutational patterns contribute positively to fitness through comparable perturbations of the secondary structure.

When replacing wild-type GAT8 with one of the three new variants in the strain used for proline auxotrophy selection strain SDT1066, an improvement in growth rate and reduction in lag phase was observed when growing the strain in the same conditions as were used to select the GAT variants (Fig. 5B). The growth rates correspond to approximately 60 % of the maximum growth rates predicted by the metabolic model (Fig. 4B), indicating potential to further increase growth and GAT activity. The model assumed a glucose uptake rate typical of *E. coli* wild-type strains and therefore did not incorporate the growth-limiting effects of genetic engineering, potentially leading to an over-estimation of growth for SDT1066. We subsequently conducted bioconversion assays, where arginine and glycine are converted into GAA by the novel GAT8 variants. This assay revealed improvements in GAA production of 90 %, 94 %, and 73 % for GAT8_v1, v2 and v3, respectively, compared with GAT8_wt (Fig. 5C). Importantly, these findings demonstrate that the growth rate increases observed in the selection experiment were directly linked to an improvement in catalytic capability of GAT.

2.9. The new GAT variants lead to improved creatine production

After obtaining better GAT variants, we continued to assemble the pathway for creatine production. Although no significant growth defect was seen when added externally (Supplementary Fig. 1), we noticed that creatine inhibits *E. coli* growth when produced intracellularly (Supplementary Fig. 7A).

To solve this problem, we designed another ALE to improve the tolerance of *E. coli* cells to creatine. Given that external creatine did not inhibit growth, likely due to transport limitation, we introduced the GAMT enzyme (SAM-dependent methyltransferase) and fed GAA so the cells can produce creatine intracellularly. One potential risk of such a design is that the cells may lose the GAMT plasmid to avoid growth inhibition by creatine. To prevent plasmid loss, we utilized a previously reported strain that couples SAM-dependent methyltransferase activity to growth (Luo et al., 2019). This strain, derived from *E. coli* BW25113, has a rewired SAM-cycle (encoded by pHM11) and is deficient of the natural cysteine synthesis; instead, cysteine is provided by the SAM cycle and SAM-dependent methylation. Without cysteine supplementation, the strain needs to maintain the GAMT plasmid to grow (Supplementary Fig. 7B).

We picked an efficient variant GAMT3 among the candidates (Supplementary Fig. 6) for the creatine tolerance ALE. We constructed the strain SDT1004 containing GAMT3 plasmid pSD158 and pHM11 that enables growth-coupling to methylation. The strain was evolved by feeding increasing concentrations of GAA (Materials and Methods) leading to improved growth during creatine production (Fig. 6A). We then cured the plasmids of selected isolates, retransformed plasmid pSD158 containing GAMT3, and monitored growth in M9 medium feeding GAA. The detailed workflow is illustrated in Supplementary Fig. 7C. The strains of evolved genome hosts demonstrated enhanced growth and tolerance to creatine (Fig. 6A). The mutations of selected ALE isolates are listed in Supplementary Table S7. GhxP may contribute to creatine reimport, but further research is needed to elucidate the

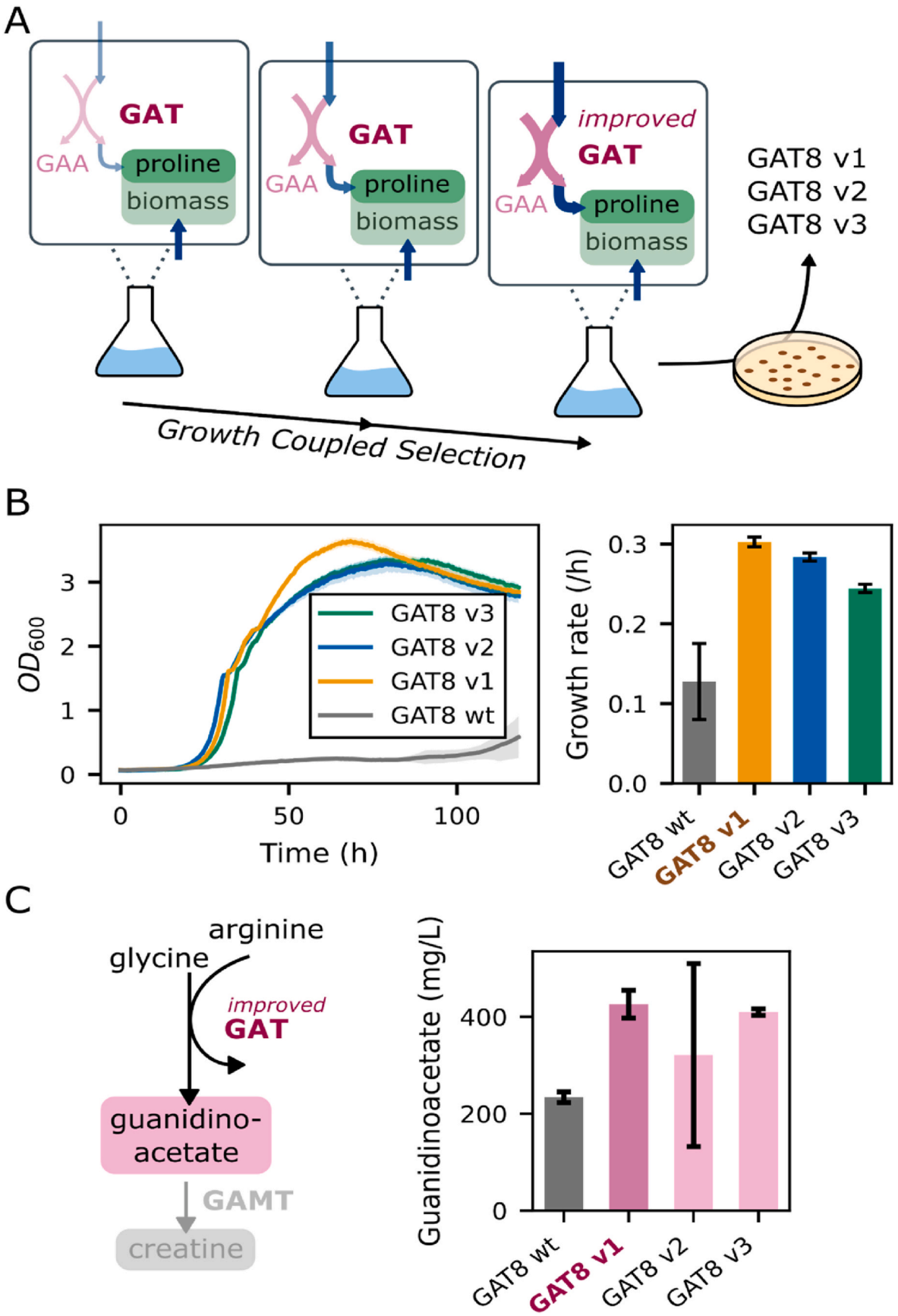

Fig. 5. A) Selection experiment using the selection system based on proline-auxotrophy. Three different GAT8 variants were isolated from this experiment. B) Growth rates of the selection system with the three recloned GAT8 variants (SDT1366-68) and GAT8-wt (SDT1156). C) GAA concentration after bioconversion of glycine and arginine using the novel GAT variants (mean±standard deviation, Materials and Methods).

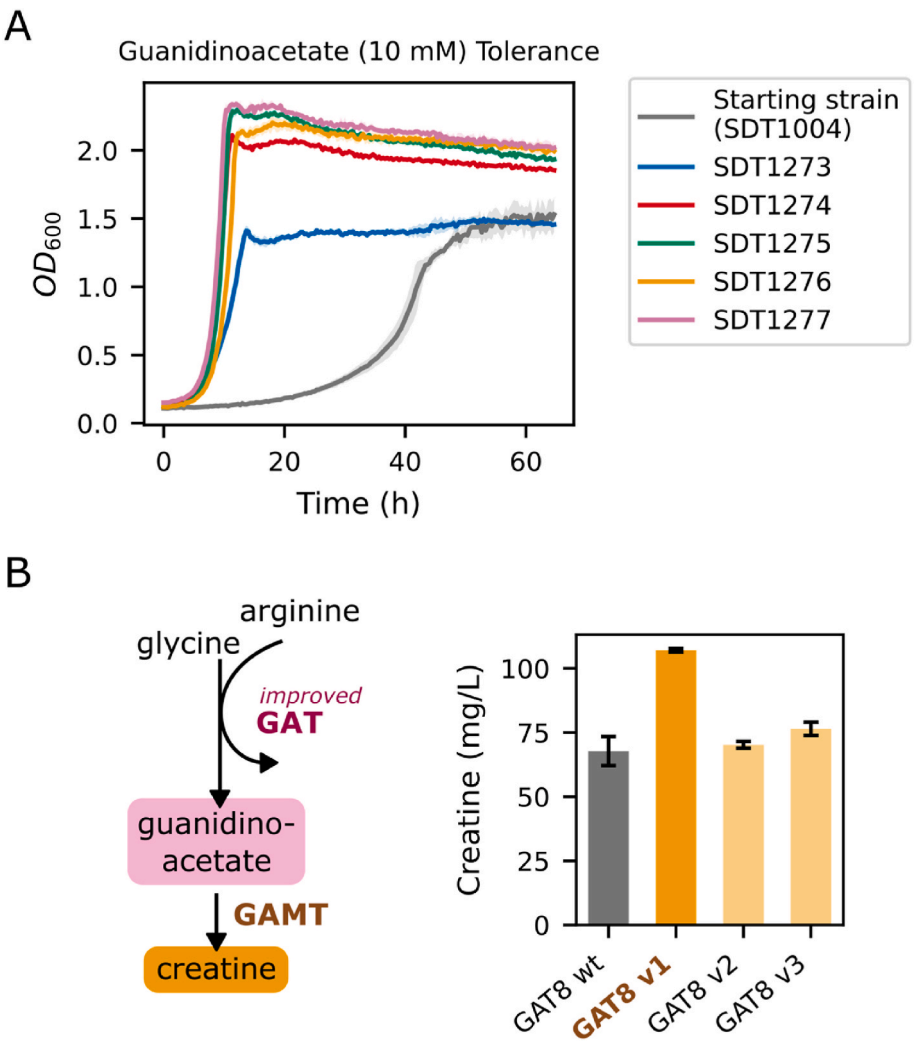

Fig. 6. Creatine production in *E. coli*. ALE isolates showed increased creatine tolerance compared to the original strain SDT1004. A). The new improved GAT variants were introduced to the evolved strain background together with GAMT. B) Extracellular creatine concentrations were then measured to demonstrate the whole-cell bioconversion of arginine and glycine to creatine. One of the variants GAT8_v1 showed more than 50 % enhancement in creatine production.

causal mutations and detailed tolerant mechanism (Supplementary Fig. 8). One of the resulting strains, SDT1243 (genome background of SDT1274 in Fig. 6A), is used as the "creatine tolerant" background.

Next, we assembled the full creatine synthesis pathway from glycine and arginine in strain SDT1243 by co-expressing GAMT4 and either GAT8_wt, GAT8_v1, GAT8_v2, GAT8_v3 in the same operon, resulting in strains SDT1373, SDT1369, 1370, and 1371, respectively (Supplementary Table S4). The four strains were used to perform whole-cell bioconversions of arginine and glycine to creatine. GAT8_v1 led to a 58 % improvement in creatine production versus GAT8_wt, reaching a titer of over 100 mg/L creatine (Fig. 6B). We further performed batch cultivation of GAT8_v1, which led to over 30 mg/L creatine after 30 h with glycine and arginine supplemented (Supplementary Fig. 11).

3. Discussion

Growth coupling is an efficient approach for pathway engineering, as it allows for the selection of improved variants by growth, eliminating the tedious analytical screening of target compounds (Alter and Ebert, 2019). Here we also demonstrated that it can be used for plasmid maintenance during creatine tolerant ALE. Additionally, as shown for methyltransferases such as GAMT, growth-coupling design can be reused for various enzymes with similar enzymatic activities. Recently, a database of enzyme selection system designs for a range of enzyme classes was published, providing a platform for several other enzyme engineering efforts (Alter et al., 2024).

Genome-scale metabolic models and algorithms have been used for *in silico* design or validation of growth-coupling (Hassani et al., 2024; Jensen et al., 2019). From a theoretical standpoint, growth-coupled production is feasible for nearly all metabolites (Von Kamp and Klamt, 2017). However, implementation of the design in experiments is often challenging. For example, enzyme promiscuity, leading to underground metabolism can lead to false positive growth and failure of coupling to the target reaction (Guzmán et al., 2015; Pandya et al., 2014). In this study, we first encountered insufficient growth on proline for the coupling to work experimentally. The incorporation of additional resource allocation constraints can potentially increase prediction fidelity of metabolic models for alternative carbon sources and genetic conditions (Alter et al., 2021). The systematic discovery of enzyme promiscuities and the incorporation of novel metabolic reactions into metabolic models will increase the robustness of computed growth-coupling designs (Domenzain et al., 2022; Guzmán et al., 2019; Monk et al., 2017; Pandya et al., 2014). Consideration of regulatory features of metabolic pathways can additionally be used to evaluate the feasibility of design solutions, *e.g.,* for uncovering inhibition of key enzymes by novel medium components. For instance, information about OCD inhibition by arginine could have streamlined the design of experiment at an early stage and speed up the establishment of the

enzyme selection system.

We observed that a weaker coupling (proline demand) was much easier to implement compared to a stronger coupling (total biomass). We speculate this is because low coupling strengths correlate with less metabolic rerouting compared to wildtype flux distributions and therefore show higher cellular fitness as shown by a model-based study (Alter et al., 2024). Further testing with additional designs is needed to determine whether it can serve as a general guideline.

In conclusion, we successfully refactored the creatine biosynthesis pathway in *E. coli* by feeding glycine and arginine, laying the foundation for replacing chemical synthesis of creatine with a more sustainable process. Instead of traditional metabolic engineering approaches, we employed growth-coupling and ALE as the primary strategy, including enhancing growth and tolerance, selection of enzyme variants, and preventing unwanted escapers. This work demonstrates the power of combining growth-coupling and ALE to overcome complex biosynthetic challenges. We believe these insights have broader implications for developing growth-coupled production in biomanufacturing.

4. Materials and Methods

4.1. Metabolic model-based analyses

An enzyme selection design for growth-coupling glycine amidinotransferase (GAT) in *E. coli* was created using the Growth-coupling-suite, which is freely accessible on Github (https://github.com/biosustain/Growth-coupling-suite) (Alter et al., 2024). Metabolic model analyses were carried out to verify the enzyme selection system design. With iML1515 (Monk et al., 2017), the latest version of a continuously curated metabolic reconstruction of *E. coli* was employed and adapted accordingly as described in the Results section. The COBRApy metabolic modeling package toolbox (version 0.20.0) in combination with the Gurobi Optimizer suite (version 9.0.0) or GLPK were used for model handling and simulations (Ebrahim et al., 2013). 2D flux space projections were computed using custom python scripts.

4.2. Cultivation

All the growth experiments were done using M9 medium that contains 1X M9 salts, 0.1 mM $CaCl_2$, 2 mM $MgSO_4$, 0.2 % glucose, 1X trace minerals solution, 1X Wolfe's vitamin solution, 25 μg/mL chloramphenicol. Supplementation is added as needed. Creatine bioconversion medium (CBM): M9 supplemented with 0.2 % L-arginine, 0.2 % L-glycine; Guanidinoacetic acid bioconversion medium (GBM): M9 supplemented with 0.2 % L-arginine, 0.2 % L-glycine, 0.05 % L-proline; Auxotrophy selection medium (ASM): M9 supplemented with 0.05 % L-arginine, 0.2 % L-glycine; Ornithine growth selection medium (OSM): M9 supplemented with 0.1 % L-arginine, 0.2 % L-glycine, 0.05 % L-proline. Overnight cultures of cysteine auxotrophic strains were supplemented with 50 mg/L L-cysteine.

Growth curves were generated by cultivating strains in a Growth Profiler 960 (Enzyscreen) using 96-well CR1496dg half-deepwell microplates. G-values were converted to OD_{600} using a calibration curve made with WT BW25113. Unless otherwise specified, strains were grown overnight in LB with appropriate antibiotics. Overnight cultures were washed in M9 medium and used to inoculate 250 μL medium in the 96-well plate to an initial OD_{600} of 0.05. The number of replicate wells was 2, 3 or 4 depending on the specific experiment. The growth profiler was set to 30 °C and 225 rpm, with pictures taken every 20 min. Unless stated otherwise, M9 medium was used for growth profiler experiments with necessary additional components.

4.3. Plasmids and strains

All strains are derived from BW25113 (Baba et al., 2006). All genes are ordered from IDT with codon optimized for *E. coli*. All plasmids are constructed using Golden Gate assembly (Engler et al., 2008) or USER cloning (Geu-Flores et al., 2007). USER Enzyme and T4 DNA ligase were ordered from NEB. All synthetic gene blocks were codon optimized for *E. coli* and ordered from IDT. Colony PCR was performed using NEB OneTaq 2X Master Mix with Standard Buffer, or NEB Q5 High-Fidelity DNA Polymerase if the PCR product was subsequently sequenced. NEB *Bsa*I-HF®v2 was used for *Bsa*I restriction, including Golden Gate reactions. Constructed plasmids were cloned into One Shot™ TOP10 Chemically Competent *E. coli* cells according to supplier instructions. Genome engineering was conducted using a CRISPR-based system described previously (Phaneuf et al., 2021). All strains, plasmids, gene sequences are listed in Supplementary Tables 1–4.

Error-prone PCR was performed according to the supplier instructions using the GeneMorph II random mutagenesis kit (Agilent Technologies). The epPCR product was gel purified and cloned into the appropriate vectors using Golden Gate assembly. To maximize the number of transformants, the Golden Gate reactions were concentrated prior to transformation. This was done by removing salts and small DNA fragments using AMPure XP Bead purification (Beckman Coulter Life Sciences), followed by elution in Milli-Q water. Populations used for selection for increased GAT activity were generated by electroporation of purified and concentrated Golden Gate reaction product into the background strain. To increase the number of distinct transformants, four transformations were performed to generate each population. For each population, after outgrowth in S.O.C. medium, recovered cells from four transformations were mixed in a 250 mL baffled Erlenmeyer flask. Serial dilutions of the mixture were plated on LB with appropriate antibiotics to estimate the number of transformed cells. The mixture was then diluted 1:3 with 2xYT, incubated 30 °C and 225 rpm for 2.5 h or overnight for amplification. The amplified population was then stored at −70 °C as glycerol stocks until its revival for the subsequent selection experiment. For GAT selection using strain SDT969, the epPCR library was constructed on the pSD221 plasmid backbone with the pSC101 origin of replication, compatible with the p15 A origin in the OCDv4-bearing plasmid. The transformed library was first grown in non-selective media (2xYT) with chloramphenicol and ampicillin, and subsequently washed and transferred to both liquid media and agar plates, with arginine and glycine as the sole carbon sources.

4.4. Auxotrophy-based growth-coupled selection

In the first round of proline auxotrophy-based selection, for each of the three populations used for selection, two vials of frozen glycerol stock with amplified population were thawed and washed twice in ASM. The washed populations were used in their entirety to inoculate 50 mL of ASM in 250 mL baffled Erlenmeyer flasks. The flasks were incubated at 30 °C and 225 rpm until OD_{600} stopped increasing, at which point the culture was used to inoculate 50 mL fresh ASM medium. After the second flask stopped growing, the culture was passed once more, resulting in a total of three flasks per selected population. The outgrown, selected population from each flask was saved and used to screen for GAT variants by streaking for single colonies on LB with chloramphenicol and ampicillin.

In the second round of auxotrophy-based selection, lysate from flask 1 of the first round was used as template for a second round of GAT epPCR. The PCR product was treated with *Dpn*I to remove template, purified, and cloned into pSD292 using Golden Gate assembly. Transformation of the resulting library, selection conditions, and number of passes to fresh media were all the same as in round 1. Glycerol cryostocks with populations sampled from selection experiments were streaked out on LB with ampicillin and chloramphenicol for colony isolation and sequencing.

4.5. Adaptive laboratory evolution (ALE)

To obtain growth on proline or ornithine, we designed several ALE

runs to achieve the target growth. First, we grew BW25113 ΔastA in M9 media supplemented with 4 g/L proline and 0.6 g/L glycerol. Glycerol was gradually reduced during evolution. The end point ALE population was transformed with OCD epPCR library and plated onto an M9 agar plate with 4 g/L ornithine as the sole carbon source. Colonies showed up after 4–5 days incubation at 37 °C. Several bigger colonies were picked and stocked. In the biggest colony, sequencing revealed four mutations (65 R- > H, 184 R- > H, 185 A- > V, 244 R- > H, OCDv4, SDT913) compared with OCD_{WT}.

Second, we performed another ALE parallel run by growing SDT652 in M9_0.6 g/L glycerol media with both Proline (4 g/L) and Ornithine (4 g/L), gradually removing glycerol (Proline_Ornithine ALE). No reproducible growth was observed in this ALE run. We plated the end point ALE culture on M9 agar plates containing 4 g/L ornithine and identified one colony that grows well on ornithine (SDT844, OCDv3).

Finally, we have also performed ALE by adapting SDT652 in M9_0.6 g/L glycerol containing ornithine (4 g/L) with gradually reduced glycerol (Ornithine ALE). However, no growth improvement was observed. All the above ALE experiments were done at 37 °C.

To address toxicity from intracellular creatine, ALE was performed on SDT1004 with the goal of increasing the strain's tolerance to extracellular GAA without eliminating conversion of GAA to creatine. Tolerance ALE was performed by culturing the strain in medium with increasing GAA concentration. Supplementing the medium with methionine enabled coupling of GAMT activity through, preventing deletion of the *GAMT* gene during evolution (Luo et al., 2019).

The GAA/creatine TALE experiment (CALE) was conducted by cultivating SDT1004 (KanR, CmR) in M9 medium supplemented with 2 g/L glucose, 2.24 g/L L-methionine and required antibiotics at 30 °C. We fed the strain with an increased level of GAA concentrations, starting from 2.2475 mM and reaching 29.653 mM after over 100 generations. To further increase the stress level, we also added creatine in the media starting from 1.07 g/L reaching 12.84 g/L at the end.

One end isolate from five parallel ALE experiments were randomly picked and cured of pHM11 and pSD158 (which may carry mutations) using the pFREE system (Lauritsen et al., 2017), yielding SDT1238, SDT1239, SDT1241, SDT1242 and SDT1243. For creatine tolerance tests compared to SDT1004, pSD158 were re-introduced to the strains. For comparing creatine production with different GAT8 variants generated by selection, SDT1243 was transformed with each variant cloned into pSD293.

4.6. Creatine assay

Whole-cell bioconversions of arginine and glycine to GAA and creatine were used to assess improvements in enzyme activity from wild-type GAT8 to selected GAT variants.

Precultures (50 ml) were grown in 250 mL baffled shake flasks overnight in 2xYT at 30 °C and 225 rpm in a MaxQ 8000 incubator (ThermoFisher). Precultures were washed once with an equal volume of 0.85 % NaCl and once with an equal volume of CBM. Before proceeding to bioconversion, a single sample of 0.9 UOD_{600} was taken from each washed preculture for intracellular GAA measurement. This pre-bioconversion sample was analyzed to ensure that minimal GAA from the preculture was carried over to the creatine bioconversion after the washing steps.

Unless otherwise specified, triplicate bioconversions were performed for each preculture by resuspending washed precultures in three separate 2 mL volumes CBM to an OD_{600} of 20 in 12 mL culture tubes. Bioconversion mixtures were incubated at 30 °C and 225 rpm for 18 h.

After bioconversion, cells were separated from supernatant by centrifugation for 5 min at 4000×*g*. Creatine content in the culture supernatant was measured using "Creatine Assay Kit" from Sigma-Aldrich (MAK079) according to the manufacturer's protocol.

In the bioconversion assay performed on SDT1369, SDT1370 and SDT1371, only a single bioconversion was performed per strain (n = 1). The creatine assay was then performed on three samples from each bioconversion tube, resulting in three technical replicates.

4.7. GAA bioconversion

Precultures were grown overnight in 2xYT at 30 °C and 225 rpm. Precultures were washed once with 0.85 % NaCl and once with GBM. Before proceeding to bioconversion, a single sample of 0.9 UOD_{600} was taken from each washed preculture for intracellular GAA measurement. This pre-bioconversion sample was analyzed to ensure that minimal GAA from the preculture was carried over to the GAA bioconversion after the washing steps.

Triplicate bioconversion was performed for each preculture by resuspending washed precultures in three separate 2 mL volumes GBM to an OD_{600} of 20. Bioconversion mixtures were incubated at 30 °C and 225 rpm for 20 h.

After bioconversion, cells were separated from supernatant by centrifugation for 5 min at 4000 g. Intracellular and extracellular GAA was measured by UHPLC-MS/MS. The wildtype GAA value presented in Fig. 5C is based on duplicates rather than triplicates because one sample was below detection limit. All other samples in Fig. 5C based on triplicates.

Ultra-high performance liquid chromatography coupled to tandem mass spectrometry (UHPLC-MS/MS) for analysing guanidinoacetic acid (GAA)

A commercial standard for guanidinoacetic acid (GAA) was purchased from Sigma Aldrich (Merck Life Science A/S, Søborg, Denmark). In addition, LC-MS grade acetonitrile (ACN) and 99 % pure formic acid (HCOOH) were purchased from VWR (Avantor, Radnor, PA, USA). A stock solution of the analyte was prepared in 20 % HCOOH to a concentration of 5.4 mg mL^{-1}. Working standard solutions of the stock solution were then prepared in H_2O. A calibration curve in the concentrations of 0.1, 0.25, 0.5, 1, 2.5, 5, 10, 25, 50, 100, 250, 500 and 1000 ng mL^{-1} was prepared in H_2O.

After cell harvest, the supernatant was transferred to a new 1.5 mL Eppendorf tube and centrifuged at 16000×*g* for 15 min. The supernatant was transferred to a new 1.5 mL Eppendorf tube and centrifuged at 16000×*g* for 15 min. The final supernatant was filtered into a new Eppendorf tube using a 0.2 μm syringe filter. Finally, the samples were diluted using a dilution factor of 1:500 before analysis. The dilution was done in two steps. First, a 1:50 dilution was created by pipetting 980 μL of H_2O and 20 μL of original sample into a glass vial. The solution was vortex mixed after which the final 1:500 dilution was prepared by pipetting 900 μL of H_2O into a glass vial and by adding 100 μL of the 1:50 diluted sample to this vial. The solution was vortex mixed before analysis.

Before analyses, the intra-cellular samples were extracted according to the following procedure: The cell pellet was washed twice in ice-cold 0.85 % NaCl. The volume of washed cell suspension, which would result in an OD_{600}-value of 1 when resuspended in 1 mL, was transferred to a new 1.5 mL Eppendorf tube and centrifuged at 5000×*g* for 5 min. The supernatant was discarded, and 300 μL of 0.1 % formic acid was added to the washed cell pellet. This results in an OD_{600} of 3. The samples were vortex mixed and sonicated in a Bioruptor® Plus sonication device for 20 cycles of 30 s ON and 30 s OFF at the HIGH setting, before they were centrifuged at 16000×*g* (4 °C) for 5 min. The supernatant was diluted 1:3 by adding 600 μL 1 % formic acid. The diluted supernatant was then filtered through a 0.2 μm syringe filter into a 1.5 mL Eppendorf tube, and finally transferred to a glass vial with an insert before analysis.

The samples were randomized after sample preparation and analyszd by ultra-high performance liquid chromatography (ExionLC, SCIEX, Framingham, MA, USA) coupled to tandem mass spectrometry (SCIEX Triple Quad 6500+, SCIEX) using electrospray ionization in positive ion mode (UHPLC-MS/MS). Selected reaction monitoring was used for quantifying GAA and declustering potential, entrance potential, collision energy and collision cell exit potential values were optimized for

each ion transition (m/z 118 → 72 and m/z 118 → 101). Nitrogen generated by an Infinity 1031 nitrogen generator (Peak Scientific Instruments Ltd, Inchinnan, Scotland, UK) is used as the ion source gas, the curtain gas and as the collisionally activated dissociation gas. The analytes were separated chromatographically before they entered the mass spectrometer. This was done using a Luna® NH_2 Column (2 mm × 100 mm, particle size 3 μm) from Phenomenex (Torrance, CA, USA) and H_2O + 0.1 % (v/v) HCOOH as eluent A and ACN + 0.1 % (v/v) HCOOH as eluent B with a flow rate of 0.35 μL min^{-1}. The elution gradient was as follows: 0–0.5 min 90 % B, 0.5–1 min 90 %–5 % B, 1–2.9 min 5 % B, 2.9–3 min 5 %–90 % B. After each run, the column was re-equilibrated at 90 % B for 3 min. The injection volume for each sample was 5 μL and the column oven temperature was maintained at 40 °C. All data was acquired and processed using the SCIEX OS software (version 3.0.0.3399).

CRediT authorship contribution statement

Jinbei Li: Methodology, Investigation, Writing – original draft. **Simon R. Krarup:** Methodology, Investigation, Formal analysis, Writing - Original Draft, Writing – review & editing. **Pascal Pieters:** Methodology, Software, Formal analysis, Visualization, Data Curation, Writing – review & editing. **Tobias B. Alter:** Writing – review & editing, Methodology, Formal analysis, Writing – original draft. **Paul Jacottin:** Formal analysis, Investigation, Validation, Writing – review & editing. **Josefin Johnsen:** Writing – review & editing, Formal analysis, Investigation. **Elsayed T. Mohamed:** Writing – review & editing, Investigation. **Thomas Harris:** Writing – review & editing, Investigation. **Linda Ahonen:** Writing – review & editing, Writing – original draft, Investigation. **Khem Bahadur Adhikari:** Writing – review & editing, Investigation. **Bernhard O. Palsson:** Writing – review & editing, Conceptualization, Funding acquisition, Supervision. **Adam M. Feist:** Writing – review & editing, Resources, Project administration, Supervision. **Lei Yang:** Writing – review & editing, Visualization, Supervision, Resources, Project administration, Conceptualization, Writing – original draft.

Protein structure visualization

Structures in Supplementary Figs. 9–10 were generated using AlphaFold3 using AlphaFold Server (Abramson et al., 2024). Generated structures were visualized using Open-Source PyMOL molecular Graphics System v.3.1.0.

Notes

During the preparation of this work the author(s) used ChatGPT in order to refine the language. After using this tool, the author(s) reviewed and edited the content as needed and take(s) full responsibility for the content of the publication.

Competing interests

JL, SK, PP, TA and LY are inventors of the patent application EP24215771.7.

Acknowledgements

This work was funded by the Novo Nordisk Foundation grant NNF20CC0035580. We thank Emre Ozdemir for discussions. We also appreciate Christina Lenhard, Christoffer Rode, Se Hyeuk Kim, Lena Elisabeth Charlotte Heer, Elina C. Olson, and Ciara De Venecia for technical support.

Appendix A. Supplementary data

Supplementary data to this article can be found online at https://doi.org/10.1016/j.ymben.2025.07.009.

Data availability

Data will be made available on request.

References

Abramson, J., Adler, J., Dunger, J., Evans, R., Green, T., Pritzel, A., Ronneberger, O., Willmore, L., Ballard, A.J., Bambrick, J., Bodenstein, S.W., Evans, D.A., Hung, C.-C., O'Neill, M., Reiman, D., Tunyasuvunakool, K., Wu, Z., Žemgulytė, A., Arvaniti, E., Beattie, C., Bertolli, O., Bridgland, A., Cherepanov, A., Congreve, M., Cowen-Rivers, A.I., Cowie, A., Figurnov, M., Fuchs, F.B., Gladman, H., Jain, R., Khan, Y.A., Low, C.M.R., Perlin, K., Potapenko, A., Savy, P., Singh, S., Stecula, A., Thillaisundaram, A., Tong, C., Yakneen, S., Zhong, E.D., Zielinski, M., Žídek, A., Bapst, V., Kohli, P., Jaderberg, M., Hassabis, D., Jumper, J.M., 2024. Accurate structure prediction of biomolecular interactions with AlphaFold 3. Nature 630, 493–500. https://doi.org/10.1038/s41586-024-07487-w.

Alter, T.B., Blank, L.M., Ebert, B.E., 2021. Proteome regulation patterns determine Escherichia coli wild-type and mutant phenotypes. mSystems 6. https://doi.org/10.1128/msystems.00625-20.

Alter, T.B., Ebert, B.E., 2019. Determination of growth-coupling strategies and their underlying principles. BMC Bioinf. 20. https://doi.org/10.1186/s12859-019-2946-7.

Alter, T.B., Pieters, P.A., Lloyd, C.J., Feist, A.M., Ozdemir, E., Palsson, B.O., Zielinski, D. C., 2024. Metabolic growth coupling strategies for in vivo enzyme selection systems. https://doi.org/10.1101/2024.09.16.613188.

Baba, T., Ara, T., Hasegawa, M., Takai, Y., Okumura, Y., Baba, M., Datsenko, K.A., Tomita, M., Wanner, B.L., Mori, H., 2006. Construction of Escherichia coli K-12 in-frame, single-gene knockout mutants: the Keio collection. Mol. Syst. Biol. 2. https://doi.org/10.1038/msb4100050.

Balestrino, M., Adriano, E., 2019. Beyond sports: efficacy and safety of creatine supplementation in pathological or paraphysiological conditions of brain and muscle. Med. Res. Rev. 39, 2427–2459. https://doi.org/10.1002/med.21590.

Bateman, A., Martin, M.-J., Orchard, S., Magrane, M., Ahmad, S., Alpi, E., Bowler-Barnett, E.H., Britto, R., Bye-A-Jee, H., Cukura, A., Denny, P., Dogan, T., Ebenezer, T., Fan, J., Garmiri, P., da Costa Gonzales, L.J., Hatton-Ellis, E., Hussein, A., Ignatchenko, A., Insana, G., Ishtiaq, R., Joshi, V., Jyothi, D., Kandasaamy, S., Lock, A., Luciani, A., Lugaric, M., Luo, J., Lussi, Y., MacDougall, A., Madeira, F., Mahmoudy, M., Mishra, A., Moulang, K., Nightingale, A., Pundir, S., Qi, G., Raj, S., Raposo, P., Rice, D.L., Saidi, R., Santos, R., Speretta, E., Stephenson, J., Totoo, P., Turner, E., Tyagi, N., Vasudev, P., Warner, K., Watkins, X., Zaru, R., Zellner, H., Bridge, A.J., Aimo, L., Argoud-Puy, G., Auchincloss, A.H., Axelsen, K.B., Bansal, P., Baratin, D., Batista Neto, T.M., Blatter, M.-C., Bolleman, J. T., Boutet, E., Breuza, L., Gil, B.C., Casals-Casas, C., Echioukh, K.C., Coudert, E., Cuche, B., de Castro, E., Estreicher, A., Famiglietti, M.L., Feuermann, M., Gasteiger, E., Gaudet, P., Gehant, S., Gerritsen, V., Gos, A., Gruaz, N., Hulo, C., Hyka-Nouspikel, N., Jungo, F., Kerhornou, A., Le Mercier, P., Lieberherr, D., Masson, P., Morgat, A., Muthukrishnan, V., Paesano, S., Pedruzzi, I., Pilbout, S., Pourcel, L., Poux, S., Pozzato, M., Pruess, M., Redaschi, N., Rivoire, C., Sigrist, C.J.A., Sonesson, K., Sundaram, S., Wu, C.H., Arighi, C.N., Arminski, L., Chen, C., Chen, Y., Huang, H., Laiho, K., McGarvey, P., Natale, D.A., Ross, K., Vinayaka, C.R., Wang, Q., Wang, Y., Zhang, J., 2023. UniProt: the universal protein knowledgebase in 2023. Nucleic Acids Res. 51, D523–D531. https://doi.org/10.1093/nar/gkac1052.

Benton, D., Donohoe, R., 2011. The influence of creatine supplementation on the cognitive functioning of vegetarians and omnivores. Br. J. Nutr. 105, 1100–1105. https://doi.org/10.1017/S0007114510004733.

Blancquaert, L., Baguet, A., Bex, T., Volkaert, A., Everaert, I., Delanghe, J., Petrovic, M., Vervaet, C., De Henauw, S., Constantin-Teodosiu, D., Greenhaff, P., Derave, W., 2018. Changing to a vegetarian diet reduces the body creatine pool in omnivorous women, but appears not to affect carnitine and carnosine homeostasis: a randomised trial. Br. J. Nutr. 119, 759–770. https://doi.org/10.1017/S000711451800017X.

Bonilla, D.A., Kreider, R.B., Stout, J.R., Forero, D.A., Kerksick, C.M., Roberts, M.D., Rawson, E.S., 2021. Metabolic basis of creatine in health and disease: a bioinformatics-assisted review. Nutrients 13, 1238. https://doi.org/10.3390/nu13041238.

Bonilla, D.A., Stout, J.R., Candow, D.G., Jiménez-García, J.D., Gómez-Miranda, L.M., Ortiz-Ortiz, M., Forbes, S.C., Ostojic, S.M., Vargas-Molina, S., Kreider, R.B., 2024. The power of creatine plus resistance training for healthy aging: enhancing physical vitality and cognitive function. Front. Physiol. 15. https://doi.org/10.3389/fphys.2024.1496544.

Brosnan, M.E., Brosnan, J.T., 2016. The role of dietary creatine. Amino Acids. https://doi.org/10.1007/s00726-016-2188-1.

Domenzain, I., Sánchez, B., Anton, M., Kerkhoven, E.J., Millán-Oropeza, A., Henry, C., Siewers, V., Morrissey, J.P., Sonnenschein, N., Nielsen, J., 2022. Reconstruction of a catalogue of genome-scale metabolic models with enzymatic constraints using GECKO 2.0. Nat. Commun. 13, 3766. https://doi.org/10.1038/s41467-022-31421-1.

Ebrahim, A., Lerman, J.A., Palsson, B.O., Hyduke, D.R., 2013. COBRApy: constraints-based reconstruction and analysis for python. BMC Syst. Biol. 7. https://doi.org/10.1186/1752-0509-7-74.

Edison, E.E., Brosnan, M.E., Aziz, K., Brosnan, J.T., 2013. Creatine and guanidinoacetate content of human milk and infant formulas: implications for creatine deficiency

syndromes and amino acid metabolism. Br. J. Nutr. 110, 1075–1078. https://doi.org/10.1017/S000711451300010X.
Engler, C., Kandzia, R., Marillonnet, S., 2008. A one pot, one step, precision cloning method with high throughput capability. PLoS One 3, e3647. https://doi.org/10.1371/journal.pone.0003647.
Feist, A.M., Zielinski, D.C., Orth, J.D., Schellenberger, J., Herrgard, M.J., Palsson, B.Ø., 2010. Model-driven evaluation of the production potential for growth-coupled products of Escherichia coli. Metab. Eng. 12, 173–186. https://doi.org/10.1016/j.ymben.2009.10.003.
Francaux, M., Poortmans, J.R., 1999. Effects of training and creatine supplement on muscle strength and body mass. Eur. J. Appl. Physiol. Occup. Physiol. 80, 165–168. https://doi.org/10.1007/s004210050575.
Geu-Flores, F., Nour-Eldin, H.H., Nielsen, M.T., Halkier, B.A., 2007. USER fusion: a rapid and efficient method for simultaneous fusion and cloning of multiple PCR products. Nucleic Acids Res. 35. https://doi.org/10.1093/nar/gkm106.
Güthner, T., Mertschenk, B., 2006. Cyanamides. In: Ullmann's Encyclopedia of Industrial Chemistry. Wiley. https://doi.org/10.1002/14356007.a08_139.pub2.
Guzmán, G.I., Sandberg, T.E., LaCroix, R.A., Nyerges, Á., Papp, H., de Raad, M., King, Z. A., Hefner, Y., Northen, T.R., Notebaart, R.A., Pál, C., Palsson, B.O., Papp, B., Feist, A.M., 2019. Enzyme promiscuity shapes adaptation to novel growth substrates. Mol. Syst. Biol. 15. https://doi.org/10.15252/msb.20188462.
Guzmán, G.I., Utrilla, J., Nurk, S., Brunk, E., Monk, J.M., Ebrahim, A., Palsson, B.O., Feist, A.M., 2015. Model-driven discovery of underground metabolic functions in *Escherichia coli*. Proc. Natl. Acad. Sci. 112, 929–934. https://doi.org/10.1073/pnas.1414218112.
Hassani, L., Moosavi, M.R., Setoodeh, P., Zare, H., 2024. FastKnock: an efficient next-generation approach to identify all knockout strategies for strain optimization. Microb. Cell Fact. 23, 37. https://doi.org/10.1186/s12934-023-02277-x.
Jensen, K., Broeken, V., Hansen, A.S.L., Sonnenschein, N., Herrgård, M.J., 2019. OptCouple: joint simulation of gene knockouts, insertions and medium modifications for prediction of growth-coupled strain designs. Metab Eng Commun 8, e00087. https://doi.org/10.1016/j.mec.2019.e00087.
Juneja, K., Bhuchakra, H.P., Sadhukhan, S., Mehta, I., Niharika, A., Thareja, S., Nimmakayala, T., Sahu, S., 2024. Creatine supplementation in depression: a review of mechanisms, efficacy, clinical outcomes, and future directions. Cureus. https://doi.org/10.7759/cureus.71638.
Kaviani, M., Shaw, K., Chilibeck, P.D., 2020. Benefits of creatine supplementation for vegetarians compared to omnivorous athletes: a systematic review. Int. J. Environ. Res. Publ. Health. https://doi.org/10.3390/ijerph17093041.
Korovljev, D., Todorovic, N., Stajer, V., Ostojic, S.M., 2021. Food creatine and DXA-derived body composition in boys and girls aged 8 to 19 years. Nutr. Metab. Insights 14. https://doi.org/10.1177/11786388211059368.
Lauritsen, I., Porse, A., Sommer, M.O.A., Nørholm, M.H.H., 2017. A versatile one-step CRISPR-Cas9 based approach to plasmid-curing. Microb. Cell Fact. 16. https://doi.org/10.1186/s12934-017-0748-z.
Li, C., Sun, P., Wei, G., Zhu, Y., Li, J., Liu, Y., Chen, J., Deng, Y., 2024. Efficient biosynthesis of creatine by whole-cell catalysis from guanidinoacetic acid in Corynebacterium glutamicum. Synth. Syst. Biotechnol. 9, 99–107. https://doi.org/10.1016/j.synbio.2024.01.003.
Li, Z., Deng, Y., Yang, G.Y., 2023. Growth-coupled high throughput selection for directed enzyme evolution. Biotechnol. Adv. https://doi.org/10.1016/j.biotechadv.2023.108238.
Long, M., Xu, M., Qiao, Z., Ma, Z., Osire, T., Yang, T., Zhang, X., Shao, M., Rao, Z., 2020. Directed evolution of ornithine cyclodeaminase using an EvolvR-Based growth-coupling strategy for efficient biosynthesis of l -Proline. ACS Synth. Biol. 9, 1855–1863. https://doi.org/10.1021/acssynbio.0c00198.
Luo, H., Hansen, A.S.L., Yang, L., Schneider, K., Kristensen, M., Christensen, U., Christensen, H.B., Du, B., Özdemir, E., Feist, A.M., Keasling, J.D., Jensen, M.K., Herrgård, M.J., Palsson, B.O., 2019. Coupling S-adenosylmethionine–dependent methylation to growth: design and uses. PLoS Biol. 17. https://doi.org/10.1371/journal.pbio.2007050.
Luo, H., Yang, L., Kim, S.H., Wulff, T., Feist, A.M., Herrgard, M., Palsson, B.Ø., 2020. Directed Metabolic Pathway Evolution Enables Functional Pterin-dependent aromatic-amino-acid Hydroxylation in Escherichia coli. ACS Synth. Biol. 9, 494–499. https://doi.org/10.1021/acssynbio.9b00488.
Monk, J.M., Lloyd, C.J., Brunk, E., Mih, N., Sastry, A., King, Z., Takeuchi, R., Nomura, W., Zhang, Z., Mori, H., Feist, A.M., Palsson, B.O., 2017. iML1515, a knowledgebase that computes Escherichia coli traits. Nat. Biotechnol. 35, 904–908. https://doi.org/10.1038/nbt.3956.
Moret, S., Prevarin, A., Tubaro, F., 2011. Levels of creatine, organic contaminants and heavy metals in creatine dietary supplements. Food Chem. 126, 1232–1238. https://doi.org/10.1016/j.foodchem.2010.12.028.
Orsi, E., Claassens, N.J., Nikel, P.I., Lindner, S.N., 2021. Growth-coupled selection of synthetic modules to accelerate cell factory development. Nat. Commun. 12, 5295. https://doi.org/10.1038/s41467-021-25665-6.
Pandya, C., Farelli, J.D., Dunaway-Mariano, D., Allen, K.N., 2014. Enzyme promiscuity: engine of evolutionary innovation. J. Biol. Chem. 289, 30229–30236. https://doi.org/10.1074/jbc.R114.572990.
Phaneuf, P.V., Zielinski, D.C., Yurkovich, J.T., Johnsen, J., Szubin, R., Yang, L., Kim, S. H., Schulz, S., Wu, M., Dalldorf, C., Ozdemir, E., Lennen, R.M., Palsson, B.O., Feist, A.M., 2021. Escherichia coli data-driven strain design using aggregated adaptive laboratory evolution mutational data. ACS Synth. Biol. 10, 3379–3395. https://doi.org/10.1021/acssynbio.1c00337.
Pischel, I., Gastner, T., 2007. Creatine-its chemical synthesis. Chem. Legal 46, 291–307.
Prokopidis, K., Giannos, P., Triantafyllidis, K.K., Kechagias, K.S., Forbes, S.C., Candow, D.G., 2023. Effects of creatine supplementation on memory in healthy individuals: a systematic review and meta-analysis of randomized controlled trials. Nutr. Rev. 81, 416–427. https://doi.org/10.1093/nutrit/nuac064.
Sandberg, T.E., Salazar, M.J., Weng, L.L., Palsson, B.O., Feist, A.M., 2019. The emergence of adaptive laboratory evolution as an efficient tool for biological discovery and industrial biotechnology. Metab. Eng. https://doi.org/10.1016/j.ymben.2019.08.004.
Schindler, U., Sans, N., Schröder, J., 1989. Ornithine cyclodeaminase from octopine Ti plasmid Ach5: identification, DNA sequence, enzyme properties, and comparison with gene and enzyme from nopaline Ti plasmid C58. J Bacteriol 171, 847–854.
Schneider, P., Mahadevan, R., Klamt, S., 2021. Systematizing the different notions of growth-coupled product synthesis and a single framework for computing corresponding strain designs. Biotechnol. J. 16. https://doi.org/10.1002/biot.202100236.
Von Kamp, A., Klamt, S., 2017. Growth-coupled overproduction is feasible for almost all metabolites in five major production organisms. Nat. Commun. 8. https://doi.org/10.1038/ncomms15956.
Wang, J., Zhang, R., Zhang, Y., Yang, Y., Lin, Y., Yan, Y., 2019. Developing a pyruvate-driven metabolic scenario for growth-coupled microbial production. Metab. Eng. 55, 191–200. https://doi.org/10.1016/j.ymben.2019.07.011.